$^{11}B+\alpha$ reaction rates and primordial nucleosynthesis

T. R. Wang, R. B. Vogelaar, and R. W. Kavanagh
W. K. Kellogg Radiation Laboratory, California Institute of Technology, Pasadena, California 91125
(Received 4 September 1990)

Total cross sections and resonance yields have been measured for the $^{11}B(\alpha,n)^{14}N$ reaction for $E_\alpha=350-2400$ keV, and for the $^{14}C(p,n)^{14}N$ reaction for $E_p=1000-1550$ keV, using 4π neutron detectors. Differential cross sections for the $^{11}B(\alpha,p)^{14}C$ reaction were measured for $E_\alpha=600-1820$ keV. A strong and narrow ($\Gamma=2.2$ eV) new resonance was found at $E_\alpha=606$ keV, with $J^\pi=\frac{7}{2}^-$ established by (α,γ) and (α,p) angular distributions. This resonance dominates the thermonuclear (α,n) and (α,p) reaction rates for $T\sim0.5\times10^9$ K. The $^{11}B(\alpha,n)$, (α,p), and (α,γ) reaction rates versus temperature are presented and compared with $^{11}B(n,\gamma)$ rates.

I. INTRODUCTION

The current understanding of fundamental interactions leads one to believe that the early Universe went through several phase transitions. The last of these transitions results from quarks and gluons condensing into hadrons; this is the quantum chromodynamics (QCD) phase transition. It is likely that the QCD transition will be observable through the residual effects of inhomogeneities induced by density fluctuations at the transition point. Witten[1] suggested that the phase transition of the quark-gluon plasma into hadrons would create isothermal baryonic-density fluctuations, or high-density "nuggets," in the early Universe. Applegate and Hogan[2] showed that nucleosynthesis would be changed if the size of these "nuggets" is such that protons would not diffuse across them before the onset of nucleosynthesis, whereas neutrons would diffuse across them. This is due to Coulomb interaction between protons, which is absent for neutrons. The detailed study of the QCD transition by Alcock, Fuller, and Mathews[3,4] suggested that the likely nucleation length scale would lie in the range that allows neutron-proton diffusive segregation. The resulting scenario involves primordial nucleosynthesis taking place in both high-density proton-rich and low-density neutron-rich regions, with distinctly different nucleosynthesis reaction sequences in each region.

It has been suggested[3-8] that such conditions could reconcile an $\Omega_b=1$ universe with big-bang nucleosynthesis and, also, enhance the production of $A>12$ isotopes several orders of magnitude above standard big-bang predictions. Initial calculations of Applegate, Hogan, and Scherrer[5] predict four orders of magnitude enhancement in the total mass fraction of heavy elements ($A>12$); however, later calculations[6-8] suggest somewhat lesser enhancement. The overproduction of ^{7}Li encountered by these models,[6-8] as compared with observations[9-11] of metal-deficient Population II stars, might be resolved by incorporating back-diffusion of neutrons at late times, as suggested by Malaney and Fowler.[8] [The ^{7}Li final yield in proton-rich regions is then strongly suppressed by $^7Be(n,p)^7Li(p,\alpha)^4He$ if a late-time neutron source is present.] Recently, Boyd and Kajino,[12] and Rebolo, Molaro, Abia, and Beckman[13] pointed out that the ^{9}Be and ^{11}B abundances predicted by this model might be measurable and could provide an independent test of inhomogeneous big-band models. The older hypothesis of production of ^{9}Be and ^{11}B by spallation could also be questioned.

Malaney and Fowler[7] give the following reaction sequence as the main line of production of $A>12$ isotopes in the neutron-rich region:

$$^1H(n,\gamma)^2H(n,\gamma)^3H(d,n)^4He(t,\gamma)^7Li(n,\gamma)^8Li(\alpha,n)^{11}B(n,\gamma)^{12}B(\beta)^{12}C(n,\gamma)^{13}C(n,\gamma)^{14}C\ .$$

The ^{14}C produced subsequently decays to ^{14}N. This reaction chain requires knowledge of these and competing reaction rates, several of which are not well studied,[14] particularly in the crucial ^{6}Li-^{9}Be region. [The $^8Li(\alpha,n)^{11}B$ reaction has been studied recently by Paradellis *et al.*[15] through its inverse reaction $^{11}B(n,\alpha)^8Li$.] Earlier work of Applegate, Hogan, and Scherrer[5] suggested that the $^{11}B(\alpha,p)^{14}C$ reaction might be important in the neutron-rich nucleosynthesis. Leakage through this and the $^{11}B(\alpha,n)^{14}N$ reaction is the focus of this work.

Previous measurements of the $^{11}B(\alpha,n)^{14}N$ reaction were made by Bonner *et al.*,[16] Van der Zwan and Geiger,[17] and Niecke *et al.*[18] for $E_\alpha>2000$ keV, well above the most crucial energy range (≤1 MeV) and in a limited angular range. The $^{11}B(\alpha,p)^{14}C$ reaction has been measured by Dayras, Switkowski, and Tombrello[19] above $E_\alpha\sim1800$ keV, while Turowiecki *et al.*[20] measured down to 900 keV. The latter work, however, only included data near 0° and 180°. In the present work total neutron yields from the $^{11}B(\alpha,n)^{14}N$ reaction were measured for

 ©1991 The American Physical Society

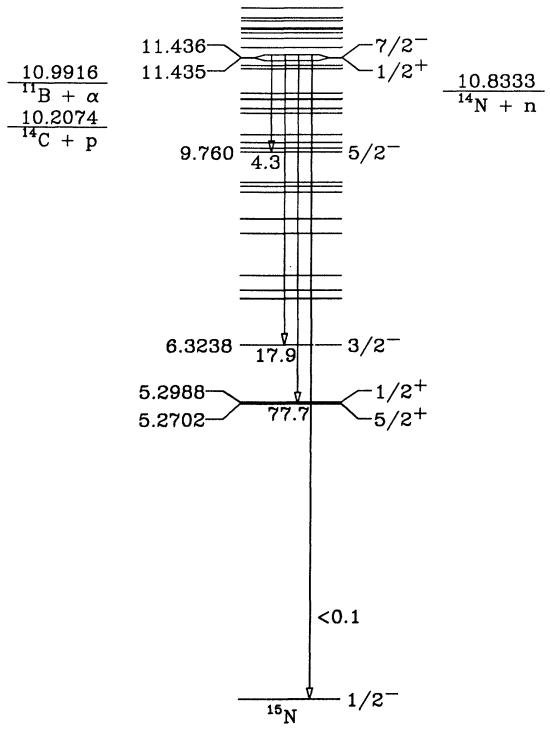

FIG. 1 Energy-level diagram of ^{15}N. The γ-ray decay scheme of the 11.436-MeV ($J^{\pi}=\frac{7}{2}^{-}$) state is also shown.

$E_{\alpha}=350-2400$ keV, using either a 4π graphite- or polyethylene-moderated neutron detector. Angular distributions for the ^{11}B$(\alpha,p)^{14}$C reaction were measured for $E_{\alpha}=600-1820$ keV, using an array of silicon-surface-barrier detectors.

A surprisingly strong narrow resonance was found in ^{11}B(α,n) at $E_{\alpha}=606$ keV, with a width much less than the beam energy spread (~ 0.2 keV), corresponding to a level at $E_x=11.436$ MeV in ^{15}N. This level was investigated in detail, through the ^{11}B(α,n), ^{11}B(α,p), ^{11}B(α,γ), and ^{14}C(p,n) reactions, in order to determine its spin, parity, and partial widths for the open n, p, α, and γ channels[21] (see Fig. 1). This resonance is found to dominate the ^{11}B(α,n) and (α,p) reaction rates in the temperature range near $T=0.5\times10^{9}$ K ($T_9=0.5$), prevailing during the nucleosynthesis epoch.

II. EXPERIMENTAL PROCEDURE AND APPARATUS

The ^{11}B$(\alpha,n)^{14}$N reaction for $E_{\alpha}>600$ keV was studied using either the JN accelerator or the JN accelerator in series with the EN tandem accelerator at Caltech. Other measurements used the Pelletron tandem accelerator. Typical beam current on the target was 10–15 μA, but ranged from as high as 30 μA to as low as 10 nA depending on counting-rate requirements and target stability. Beam energy was determined to better than 0.1% by a 90° analyzing magnet, calibrated using known resonances in the ^{14}C$(p,n)^{14}$N reaction, the 1530.03-keV resonance in the ^{24}Mg$(\alpha,\gamma)^{28}$Si reaction, and the 991.88-keV resonance in the ^{27}Al$(p,\gamma)^{28}$Si reaction.

Several ^{11}B and ^{14}C targets were used in the experiments, as described in Sec. III.

A. Neutron detection

Neutron yields from ^{11}B$(\alpha,n)^{14}$N and ^{14}C$(p,n)^{14}$N reactions were measured using 4π moderated neutron detectors (graphite at the EN tandem and polyethylene at the Pelletron). A detailed description of the detectors is given elsewhere.[22,23]

The graphite cube was $140\times141\times146$ cm^3; the polyethylene cube, $40\times40\times40$ cm^3, was Cd wrapped, with additional polyethylene and paraffin placed outside for further background reduction (to 0.1 counts/s). The thermalized neutrons were detected through the ^{3}He$(n,p)^3$H reaction using 12 embedded ^{3}He-filled proportional counters. Cosmic-ray-induced neutron events in the polyethylene cube could be vetoed using a 2.54-cm-thick, 2π array of plastic-scintillator paddles, to achieve a background rate of 0.03 counts/s. With a calibrated ($\pm3\%$) ^{252}Cf source, the efficiency of the graphite cube was determined to be 12.3% and of the polyethylene cube to be 22.2%. Using the known neutron yield from the ^{7}Li$(p,n)^7$Be reaction, the neutron detection efficiency of both detectors was found to be constant to $\pm5\%$ from 50-kV to 2-MeV neutron energy.

The beam spot on the target was defined by a water-cooled collimator of 4.8-mm diameter, followed by a 6.4-mm beam wipe and a -400-V suppressor. The vacuum in the vicinity of the target was $\sim7\times10^{-7}$ torr. A beam-profile monitor, located immediately prior to the collimator, facilitated deliberate defocusing of the beam. When required, the target was directly water cooled to prevent overheating. A 0–20-kV linear sawtooth ramping voltage was applied to the target chamber when searching for narrow resonances in the ^{14}C$(p,n)^{14}$N reaction. This in effect varied the incident beam energy, while leaving the accelerator settings unchanged.

B. Charged-particle detection

The angular distribution for the ^{11}B$(\alpha,p)^{14}$C reaction was measured in a scattering chamber, using eight 100-μm-thick surface-barrier detectors located at 0°, 20°, 40°, 70°, 90°, 120°, 140°, and 160° with respect to the beam direction. Another detector was put at the opposite side at 90° to check left-right asymmetry of the assembly. The distance between target and detectors was 13 cm, and each detector subtended a solid angle of 9.7 msr. Nb foil with proper thickness (2–4μm) was put in front of the detectors to stop the scattered beam particles.

Two beam collimators, at 5.5 and 11.6 cm upstream from the target, were used to define the beam position on the target. The diameter of upstream collimator was 1.6 mm and that of the downstream collimator 3.2 mm. In order to suppress secondary electrons from the collimator, a ring biased at -400 V was put between the downstream collimator and target, and the target was biased at $+300$ V.

The target ladder was electrically insulated from the chamber to allow for current integration. For runs with

a transparent target, current was measured with a graphite Faraday cup placed downstream at 0°.

C. Gamma-ray detection

The angular distribution for the $^{11}B(\alpha,\gamma)^{15}N$ reaction was measured using a 35% high-purity germanium detector, with an energy resolution at 1.33 MeV of 3.4 keV. The beam-line arrangement was similar to that used in the neutron detection. The distance between the target and Ge detector face was 4 cm for the angular distribution measurement and 0.6 cm for integrated yields (with the detector at 0°). In the latter geometry the relative detector efficiency[24] for 0.4–10-MeV γ rays was determined using the known decay scheme of a ^{56}Co source, the cascade scheme of the 992-keV resonance in $^{27}Al(p,\gamma)^{28}Si$, and the direct-capture γ-ray cascade from the $^{16}O(p,\gamma)^{17}F$ reaction. Absolute normalization[24] was made to a National Bureau of Standards source.

D. Instrumentation

Data from the $^{11}B+\alpha$ reactions were stored as 4- or 8-K spectra. Dead time, as determined with a pulser, was always less than 20%, and in most cases $\leq 5\%$. When data were taken with the target chamber biased by the ramp voltage, a separate analog-to-digital converter was used to monitor the ramp voltage during data acquisition. In this case the observed pulser rate versus ramp voltage was used to check for any nonlinearity in the ramp voltage (always linear to within 0.5%). In addition, possible corona and leakage currents due to the high voltage were monitored and corrected for by binning the integrated charge against the ramp voltage.

III. REACTION MEASUREMENTS AND RESULTS

A. $^{11}B(\alpha,n)^{14}N$ reaction

The targets used in the $^{11}B(\alpha,n)$ reaction were made by vacuum evaporation of 98.1% enriched ^{11}B onto a 0.25-mm-thick W backing. Yields were normalized to a ^{11}B target evaporated onto a Si crystal (oriented to minimize backscattering from the silicon) whose thickness and stoichiometric composition were determined from elastic scattering of 2-MeV α particles at 170°. (The scattering at this angle was experimentally verified to be consistent with Rutherford scattering to within 5%.) This calibrated target was composed of 4.26 ± 0.25 $\mu g/cm^2$ ^{11}B and 1.45 ± 0.09 $\mu g/cm^2$ ^{16}O. Other targets were normalized to this one by comparing neutron yields at $E_\alpha=1.05$ MeV where the cross section is relatively flat and/or by measuring the thick-target yield of the narrow resonance at 606 keV. The present normalization gives a cross section at $E_\alpha=2064$ keV, ~19% higher than that of Morgan[25] as determined by reciprocity from the inverse reaction $^{14}N(n,\alpha_0)^{11}B$. Most of the data were taken using a target having 3.4 ± 0.2 $\mu g/cm^2$ of ^{11}B. For $E_\alpha \leq 600$ keV a 37 ± 4-$\mu g/cm^2$ ^{11}B target was used.

The measured cross section for $^{11}B(\alpha,n)^{14}N$ is converted to the astrophysical S factor using

$$\sigma(E)=\frac{S(E)}{E}\exp(-2\pi\eta)\ , \tag{1}$$

where $2\pi\eta=2\pi Z_1Z_2/\hbar v=[287.34\ \text{MeV}/E]^{1/2}$, Z_1,Z_2 are charges of the incident particle and target, and v is the relative velocity. The S factor versus center-of-mass energy E of the $^{11}B(\alpha,n)^{14}N$ reaction is shown in Fig. 2.

The cross section of the $^{11}B(\alpha,n)^{14}N$ reaction from $E_{c.m.}=820$ to 1800 keV was fitted with a linear background and six independent Breit-Wigner resonances. These included a weak resonance at $E_{c.m.}=1327$ keV and a broad resonance ($\Gamma_{c.m.}=400$ keV) at 1069 keV, but excluded the narrow resonance at 950 keV. The result is shown as the solid curve in Fig. 2. The resulting resonance widths, locations, and strengths are listed in Table I. The cross section from $E_{c.m.}=400$ to 820 keV cannot be fitted by two isolated resonances. The skewness of the cross section near 700 keV indicates either that the $E_{c.m.}=770$ keV $\frac{3}{2}^+$ resonance interferes with another broad resonance with the same J^π or that there is an additional resonance at ~730 keV. Because of the absence of a known broad nearby $\frac{3}{2}^+$ resonance, the cross section from 400 to 820 keV, excluding the contribution from the 444.4-keV narrow resonance, was fitted with two independent Breit-Wigner resonances, plus a hypothetical broad resonance ($\Gamma_{c.m.}=188$ keV) at 730.4 keV and a linear background. The result is also shown as a solid curve in Fig. 2, and the resonance parameters are included in Table I.

The strength and J^π of the resonance at $E_{c.m.}=444.4$ keV ($E_x=11.436$ MeV), which is important in the temperature range of primordial nucleosynthesis, have not been studied previously in this reaction channel. The neutron yield of this resonance, measured with both thin and moderately thick targets, is shown in the inset in Fig. 2. The resonance strength $(\omega\gamma)_{c.m.}$ of this narrow resonance can be determined from the step height Y of the thick-target yield as

$$(\omega\gamma)_{c.m.}=\frac{2\epsilon}{\lambda^2}\frac{M}{M+m}Y\ , \tag{2}$$

where ϵ is the stopping power of helium in ^{11}B in the laboratory system, λ is the center-of-mass de Broglie wavelength, and M and m are the masses of the target and projectile, respectively. The stopping power was taken from the compilation of Ziegler.[26] A thick ^{11}B target (~85 keV) was used to measure the step height of the 444-keV ($E_\alpha=606$ keV) resonance and is shown in Fig. 3(a). The target was prepared to minimize exposure to air, and the oxygen content of the target was negligible. The step height of this resonance (subtracting out the contribution of the underlying broad resonance) was 28 counts/μC. Using the detector efficiency of 22.2% (see Sec. II A), the strength of the resonance was determined to be $(\omega\gamma)_{c.m.}=(0.175\pm0.010)$ eV. The determination of J^π for this resonance is described in Secs. III B and III C.

The same ~85-keV-thick ^{11}B target was used to study the $E_\alpha=411$ keV resonance. The excitation function is shown in Fig. 3, along with a fit to the low-energy tail of the $E_\alpha=605$ keV, $J^\pi=\frac{1}{2}^+$, resonance. The net yield of

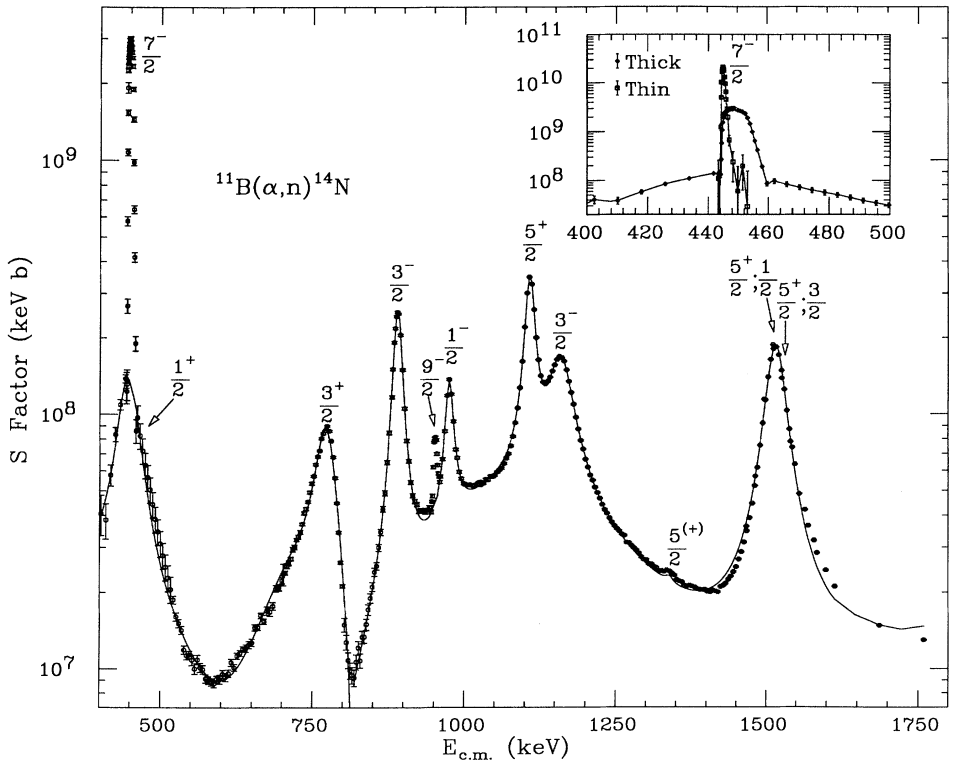

FIG. 2. S factor versus center-of-mass energy for the ^{11}B$(\alpha,n)^{14}$N reaction. The solid line above 820 keV represents a fit using six Breit-Wigner resonances plus a linear background, while the solid line below 820 keV represents a fit to the S factor using three Breit-Wigner resonances plus a linear background (see text). The solid lines in the inset are just a link of data points. The $J^{\pi};T$ assignments of the resonances are from Ajzenberg-Selove (Ref. 21), except for the $\frac{7}{2}^-$ state determined in the present work.

TABLE I. Resonances in the ^{11}B$(\alpha,n)^{14}$N reaction.

No.	E_α (keV)[a]	$E_{c.m.}$ (keV)	J^{π}[b]	$\Gamma_{c.m.}$ (keV)	$(\omega\gamma)_{c.m.}$ (eV)	E_x (keV)
1	336.7±1.4[c]	246.9±1.0	$\geq 3/2$			11 238.5±1.0
2	411.0±2.0[d]	301.4±1.5	$\frac{1}{2}^-$	<10[d]	$(16\pm2)\times10^{-6}$	11 293.0±1.5
3	604.7±1.0	443.5±0.7	$\frac{1}{2}^+$	38.2±4.0	$(55\pm4)\times10^{-3}$	11 435.1±0.7
4	606.0±0.5	444.4±0.4	$\frac{7}{2}^-$	$(2.5\pm0.5)\times10^{-3}$	0.175±0.010	11 436.0±0.4
5	(996.0±1.5)[e]	(730.4±1.1)		(188±2)	(22±2)	(11 722.0±1.1)
6	1049.4±1.0	769.6±0.7	$\frac{3}{2}^+$	41.0±0.5	15±1	11 761.2±0.7
7	1209.7±1.0	887.2±0.7	$\frac{3}{2}^-$	17±3	70±11	11 878.8±0.7
8	1293.2±1.0	948.4±0.7	$\frac{9}{2}^-$	<1.5	3.1±0.2	11 940.0±0.7
9	1326.2±1.0	972.6±0.7	$\frac{1}{2}^-$	15±2	56±8	11 964.2±0.7
10	1458.1±6.4	1069.3±4.7		400±33	$(2.0\pm0.2)\times10^{3}$	12 060.9±4.7
11	1507.2±1.0	1105.3±0.7	$\frac{5}{2}^+$	17.4±0.4	$(0.57\pm0.03)\times10^{3}$	12 096.9±0.7
12	1577.1±1.0	1156.6±0.7	$\frac{3}{2}^-$	48.0±0.5	$(0.93\pm0.06)\times10^{3}$	12 148.2±0.7
13	1823.2±1.0	1337.1±0.7	$\frac{5}{2}^+$	14±3	8±2	12 328.7±0.7
14	2063.7±1.0	1513.5±0.7	$\frac{5}{2}^+$	39±4	$(7.9\pm0.7)\times10^{3}$	12 505.1±0.7

[a]Except for the 606-keV resonance, energies listed are the observed peak energies less half the target thickness.
[b]From Ref. 21, except for No. 4.
[c]From ^{14}C$(p,n)^{14}$N data; $\Gamma_{c.m.}=2.4\pm0.5$ keV.
[d]$E_\alpha=409.5\pm1.0$ keV, $E_x=11\,291.9\pm1.0$ keV, $\Gamma_{c.m.}=5.8\pm0.3$ keV from ^{14}C$(p,n)^{14}$N data.
[e]This resonance has not yet been observed before, but was found necessary in fitting the data of Fig. 2.

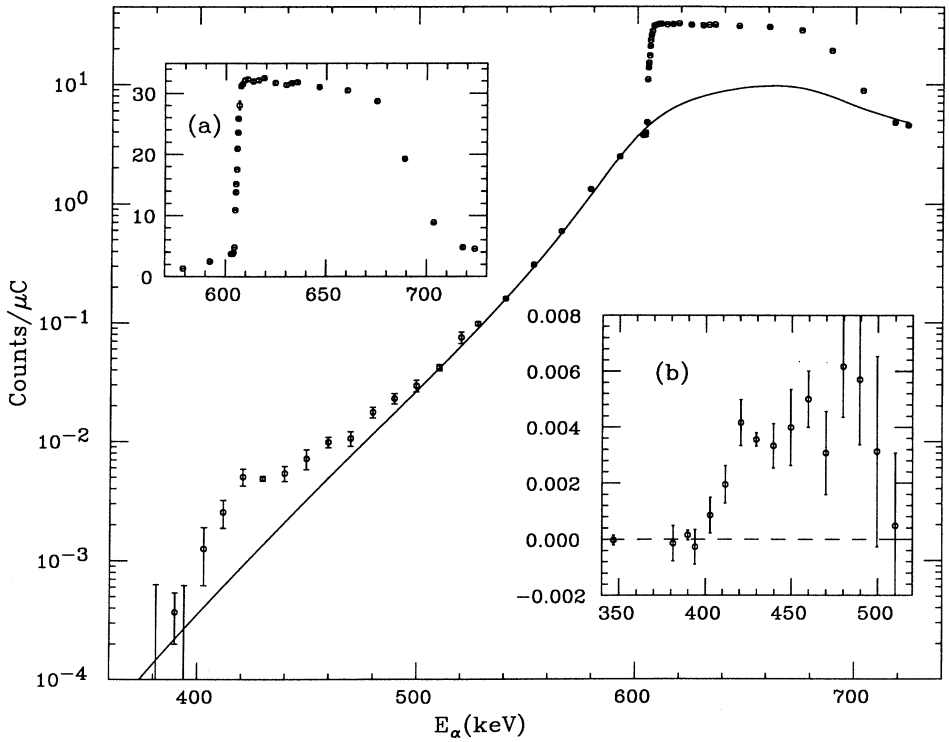

FIG. 3. Thick-target yield measurement of the $E_\alpha=411$, 605, and 606 keV resonance in the $^{11}B(\alpha,n)^{14}N$ reaction. The solid line is the fit to the 605-keV resonance folded with the target profile and penetration factor. (a) Linear plot of the thick-target profile of 606-keV resonance. (b) The net counts/μC from the 411-keV resonances after subtraction of the contribution from the 605-keV resonance.

the 411-keV resonance after background subtraction is shown in Fig. 3(b). From the relative step height of the thick-target yields at the 411- and 606-keV resonances, the strength of the $E_\alpha=411$ keV resonance was determined to be $(\omega\gamma)_{\text{c.m.}}=(16\pm2)$ μeV.

The strength of the $E_\alpha=605$ keV resonance was measured using the (3.4±0.2)-μg/cm^2 ^{11}B target (Fig. 2). From the integrated area of the low-energy tail of the 605-keV resonance from 550 to 605 keV (related to half the resonance strength), the strength was determined to be $(\omega\gamma)_{\text{c.m.}}=(55\pm4)$ meV.

B. $^{11}B(\alpha,\gamma)^{15}N$ reaction

The γ-ray angular distribution of the $E_\alpha=606$-keV ($E_x=11.436$ MeV) resonance in the $^{11}B(\alpha,\gamma)^{15}N$ reaction was measured above the resonance step (and also below for background), using a thick target of ^{11}B powder pressed into a recess in a Cu disk. The leading-edge profile of this pressed target is shown in Fig. 4. A typical γ-ray spectrum obtained above the resonance step is shown in Fig. 5. The γ-ray decay scheme of the resonance is included in Fig. 1, and the branching ratios are given in Table II. This resonance decays mainly to the 5.270-MeV ($\frac{5}{2}^+$) and 6.324-MeV ($\frac{3}{2}^-$) states in ^{15}N, with a weaker branch (~4.3%) to the 9.76-MeV ($\frac{5}{2}^-$) state and none to the ground state (<0.1%).

Gamma-ray spectra were taken at 0°, 20°, 40°, 60°, and 90° with respect to the beam direction. The angular dependence of the detection efficiency was determined using the well-known isotropic 340-keV resonance in the $^{19}F(p,\alpha\gamma)^{16}O$ reaction (target CaF_2 on similar copper backing). Corrections due to the variation of the detector efficiency with angle were ≤11%. Cascade-summing corrections were ≤13%.

The angular distributions of the resonance capture to the 5.270- and 6.324-MeV states, corrected for center of mass and angular attenuation, are shown in Fig. 6. Also shown in the figure are the calculated fits with several possible J^π assignments for the resonance. [$J^\pi=\frac{1}{2}^\pm$ or $\frac{3}{2}^-$, which would give isotropic distributions, are clearly excluded by the anisotropy of the data. For $J^\pi=\frac{3}{2}^+$ no acceptable fit is possible with $l=1$ in the entrance channel. With $l=3$ acceptable fits obtain, but the channel width $\Gamma_\alpha=0.11\pm0.03$ eV, as deduced below, would then be 5 times the Wigner limit for $R=5.4$ fm channel radius; the observed limit for the ground-state transition would imply an $E1$ strength less than 3×10^{-7} W.u.; and the $^{14}N+n$ s-wave channel would be remarkably inhibited. Also, in that case, a poor fit $\chi^2=110$ results for the (α,p) angular distribution shown in Fig. 10 below. The spin is thus determined to be $\frac{7}{2}$, which is consistent with the γ-ray branching. Combined with the data from the (α,p) reaction (Sec. III C), the parity is determined to be negative.

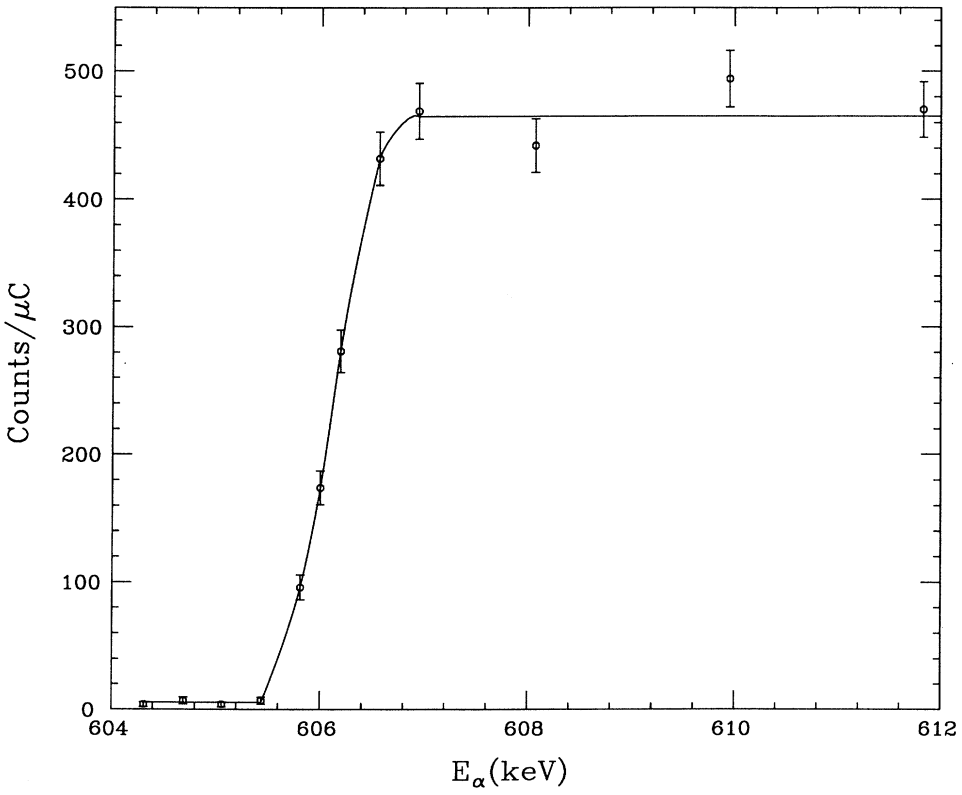

FIG. 4. Leading-edge profile of the thick target used in the measurements of the $^{11}B(\alpha,\gamma)^{15}N$ reaction.

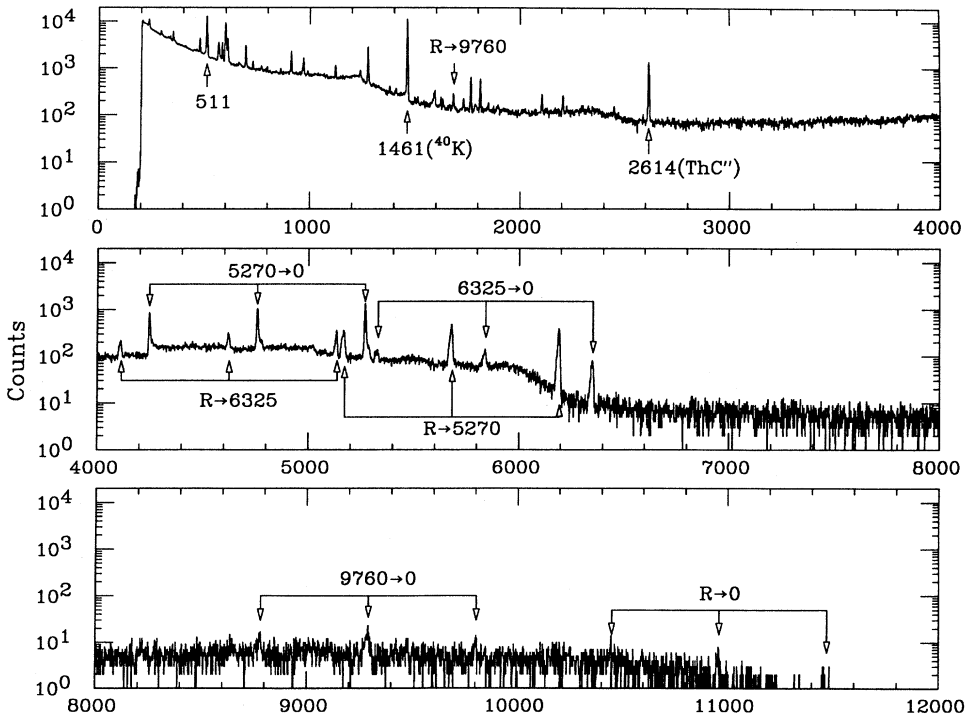

FIG. 5 Gamma-ray spectrum from the $^{11}B(\alpha,\gamma)^{15}N$ resonance at $E_\alpha = 606$ keV, taken with the Ge spectrometer at $\theta = 0°$.

TABLE II. γ-ray branching ratios of the E_x=11.436-MeV ($J^\pi=\frac{7}{2}^-$) state in ^{15}N.

E_x (MeV)	J^π	Branching ratio (%)	Γ_γ (W.u.)[a]
9.760	$\frac{5}{2}^-$	4.3±1.0	(88±31)×10^{-3}[b]
6.325	$\frac{3}{2}^-$	17.9±1.3	5.8±1.5
5.270	$\frac{5}{2}^+$	77.7±4.0	(1.6 ±0.4)×10^{-3}
0.0	$\frac{1}{2}^-$	<0.1[c]	<40

[a]The partial γ-ray widths in Weisskopf units (W.u.), using Γ_γ(total)=0.2 eV from Table VI and assuming only the lowest allowed multipoles occur.
[b]Assuming $M1$ only; the angular distribution actually indicates significant $E2$ admixture.
[c]The observed weak $R\rightarrow 0$ peaks in Fig. 5 are attributed to cascade summing.

The absolute strength of the E_α=606 keV (α,γ) resonance was determined using the step height of the thick-target yield with the detector at 0° in the close geometry described in Sec. II C, with the result, $(\omega\gamma)_{\text{c.m.}}$= (21±1) meV.

C. ^{11}B $(\alpha,p)^{14}$C reaction

The angular distribution and cross section of the ^{11}B$(\alpha,p)^{14}$C reaction was measured between E_α=600 and 1820 keV in energy steps of 20 keV, using a 49-μg/cm^2 ^{11}B target evaporated onto a 2-μm-thick Nb foil. A typical spectrum of the ^{11}B(α,p) reaction is shown in Fig. 7. Although ^{10}B constituted less than 2% of the target, the charged-particle yields for the reactions ^{10}B$(\alpha,p_i, i\leq 3)$ and ^{10}B(α,d_0) were frequently comparable to the ^{11}B(α,p_0) yield, especially at backward angles. The contribution of yields from ^{10}B was determined using a ^{10}B target (93.3% enriched ^{10}B evaporated onto 2-μm Nb), with thickness similar to the ^{11}B target, permitting subtraction to ^{10}B contaminant peaks from the spectrum of the ^{11}B$(\alpha,p)^{14}$C reaction before final analysis.

The angular distribution, after correction for center-of-mass motion and angular attenuation, was fitted by an expansion in Legendre polynomials of the form

$$\left[\frac{d\sigma}{d\Omega}\right]_{\text{c.m.}} = \sum_{i=0}^{4} a_i P_i(\cos\theta_{\text{c.m.}}) \; ; \qquad (3)$$

the total cross section is then $\sigma_t=4\pi a_0$. Higher-order terms were not required to fit the data. The resulting angular distribution coefficients and the total cross section are shown in Figs. 8 and 9, respectively. From the step height of the thick-target yield (Fig. 9), the strength of the E_α=606 keV resonance is determined to be $(\omega\gamma)_{\text{c.m.}}$=(16±1) meV. For the 604.7-keV resonance, $(\omega\gamma)_{\text{c.m.}}$=(7.9±3.2) meV is found from the integrated area of the low-energy tail of the resonance, i.e., from the average of the lowest two points in Fig. 9, which for this target thickness essentially span the lower half of the resonance yield.

The S factor for the ^{11}B$(\alpha,p)^{14}$C reaction from E_α=900 to 1800 keV was fitted with five known resonances, represented as simple Breit-Wigner forms folded with the target profile. Then the cross sections were recovered from the S factor, with the results shown as the solid curve in Fig. 9. The extracted resonance parameters are listed in Table III. The cross sections from the

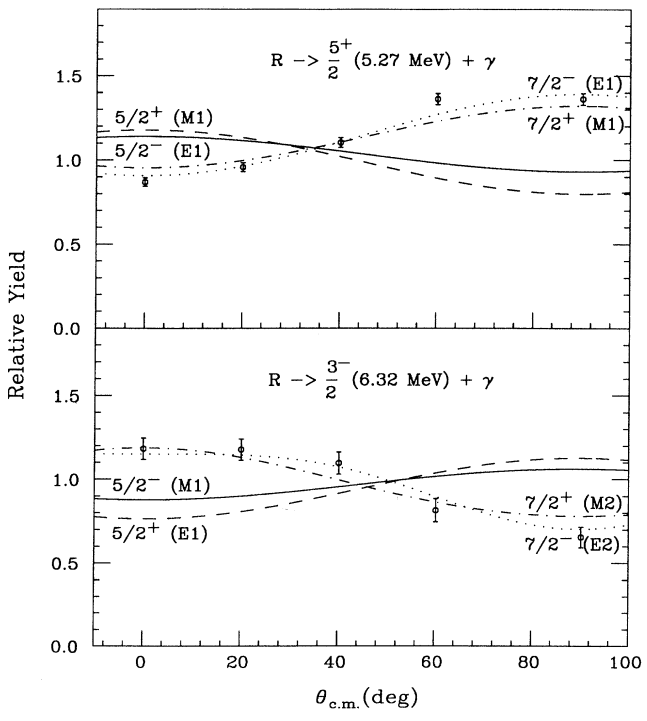

FIG. 6. Gamma-ray angular distributions of the 606-keV resonance capture to the 5.27-MeV ($\frac{5}{2}^+$) and 6.32-MeV ($\frac{3}{2}^-$) states. Shown in the figure are angular distribution fits for several possible J^π assignments to this 606-keV resonance state.

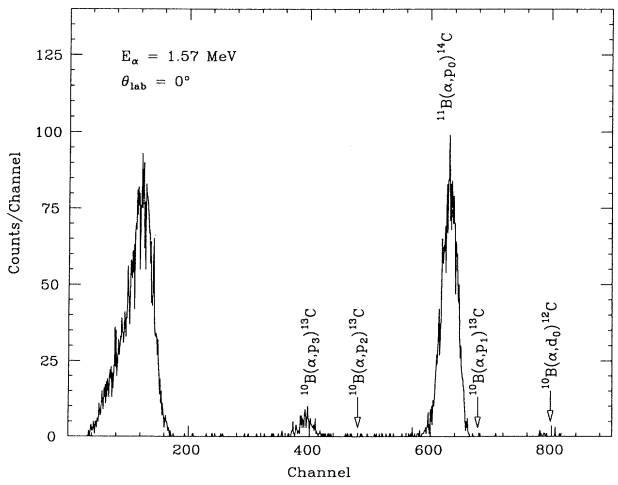

FIG. 7. Typical charged-particle spectrum from the ^{11}B+α reaction, taken with the Si detector at θ=0°. The structure below channel 180 is an artifact of the background and detector noise above the bias.

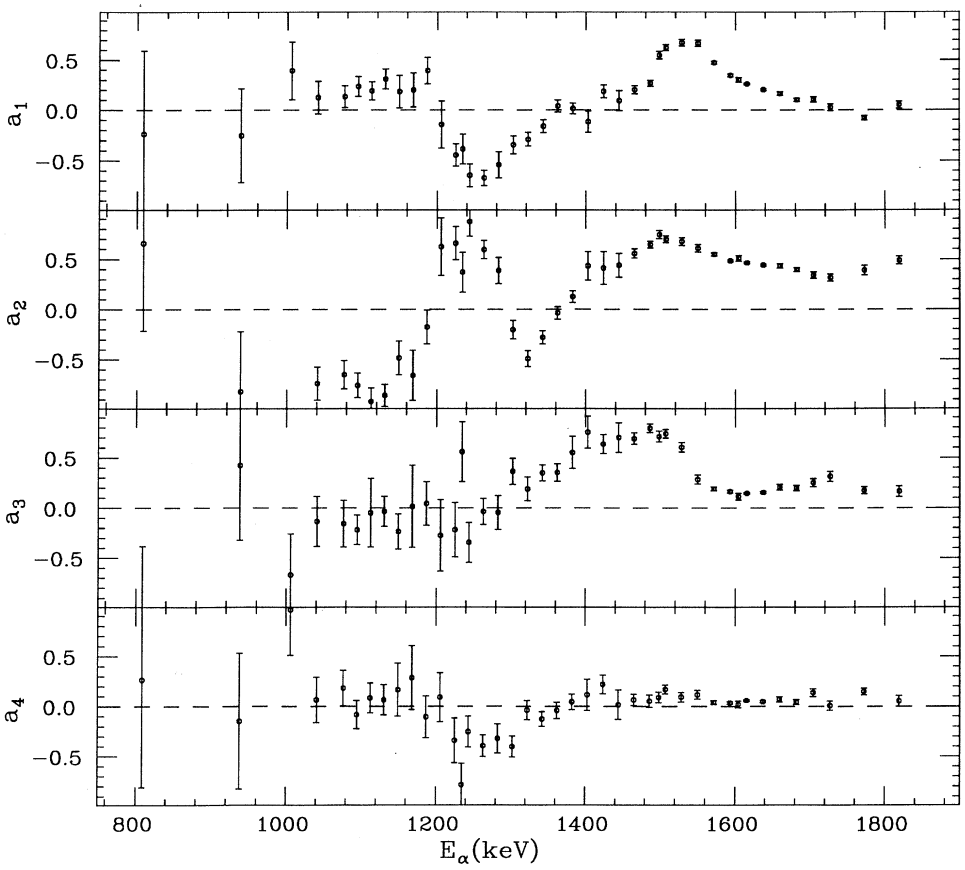

FIG. 8. Angular distribution coefficients α_k vs α energy for the $^{11}B(\alpha,p)^{14}C$ reaction.

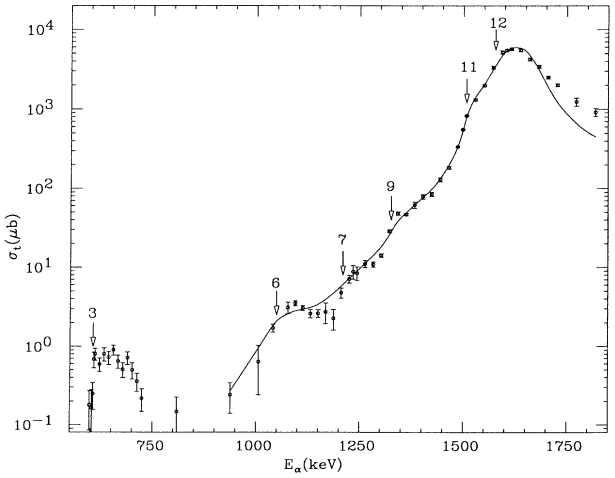

FIG. 9. Total cross section vs α energy for the $^{11}B(\alpha,p)^{14}C$ reaction. The locations of several resonances observed in the $^{11}B(\alpha,n)^{14}N$ reaction are also shown by the arrows, labeled with the resonance numbers from Table I. The solid line represents a fit to the cross section using five Breit-Wigner resonances, folded with target thickness as described in the text.

present measurements are consistent with previous work of Turowiecki *et al.*[20]

In order to determine the J^π of the $E_\alpha = 606$ keV resonance, a detailed study of the (α,p) angular distribution was performed with a single Si detector ($\Delta\Omega = 9.7$ msr) on

TABLE III. Resonances in the $^{11}B(\alpha,p)^{14}C$ reaction.

No.[a]	E_α (keV)	$\Gamma_{c.m.}$ (keV)	$(\omega\gamma)_{c.m.}$ (eV)
3	604.7[b]		$(7.9\pm3.2)\times10^{-3}$
4	606.0±0.5		$(16\pm1)\times10^{-3}$
6	1012±8[c]	41[b]	$(44\pm8)\times10^{-3}$
7	1209.7[b]	17[b]	d
9	1326.2[b]	15[b]	0.51±0.08
11	1507.2[b]	17.4[b]	39±8
12	1577.1[b]	44±2	420±20

[a]Resonances numbers as in Table I.
[b]Fixed, taken from Table I.
[c]Energy determined from the fit with Breit-Wigner shapes folded with target profile. The disagreement with the energy in Table I is attributed to the poor fit in this region, including the dip near $E_\alpha = 1150$ keV, observed also in Ref. 20.
[d]Not well defined in fit, arbitrarily fixed at 9×10^{-3}.

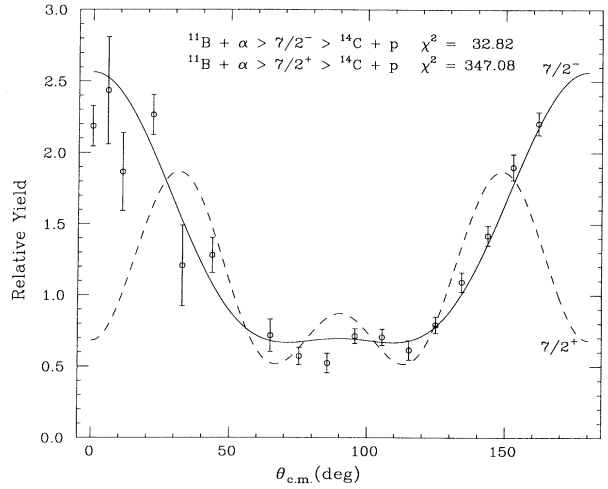

FIG. 10. Proton angular distribution from the $^{11}B(\alpha,p)^{14}C$ reaction at the $E_\alpha=606$-keV resonances. The solid and dashed lines are fits with J^π of the resonance state taken to be $\frac{7}{2}^-$ and $\frac{7}{2}^+$, respectively.

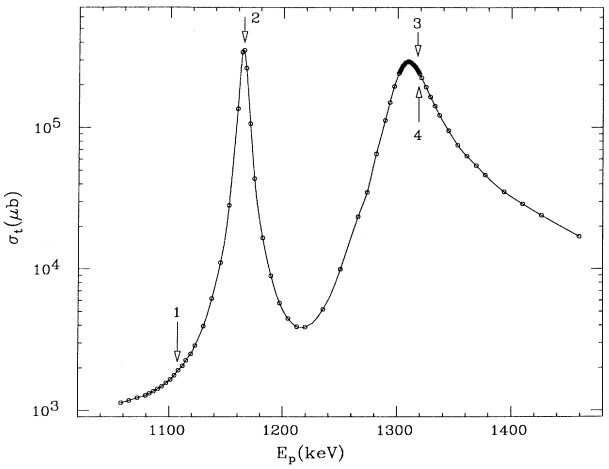

FIG. 12. Cross section versus proton energy for the $^{14}C(p,n)^{14}N$ reaction. The solid line is just a link of data points. The arrows indicate the expected positions of resonances as listed in Table I.

a rotating arm. The forward-angle measurements were made using either a self-supporting transparent ^{11}B target (30 ± 10 $\mu g/cm^2$ thick) or a ^{11}B target evaporated onto 2-μm-thick Nb foil. For backward-angle measurements, either a 7.7-$\mu g/cm^2$-(16-keV) thick ^{11}B target evaporated onto a 0.25-mm-thick W backing or the pressed ^{11}B target (see Sec. III B) were used. The relative thick-target yields from different targets were normalized at 90°. The angular distribution obtained is shown in Fig. 10, along with calculated angular distributions with J^π of the resonance set to be either $\frac{7}{2}^+$ or $\frac{7}{2}^-$ as deduced from the (α,γ) reaction. The $E_\alpha=606$ keV resonance is thus determined to have $J^\pi=\frac{7}{2}^-$.

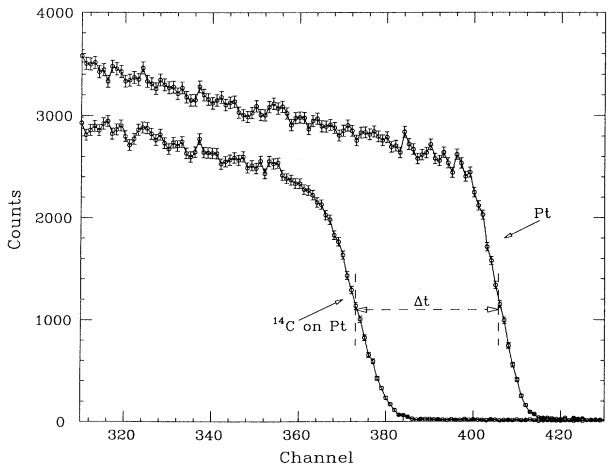

FIG. 11. Spectrum of scattered 1-MeV α's from the ^{14}C target (on Pt backing) and from the Pt backing at $\theta=170°$. The shift of the leading edge is due to the energy loss of α particles in ^{14}C determining the target thickness

D. $^{14}C(p,n)^{14}N$ reaction

A ^{14}C target (>95% enriched) on a 0.25-mm-thick Pt backing was determined to have a thickness of 20.8 ± 1.3 $\mu g/cm^2$ using elastic scattering of α's at 1 and 1.5 MeV, as illustrated in Fig. 11. The polyethylene-cube system (Sec. II A) detected the neutron yield from the $^{14}C(p,n)^{14}N$ reaction. Data were taken for proton ener-

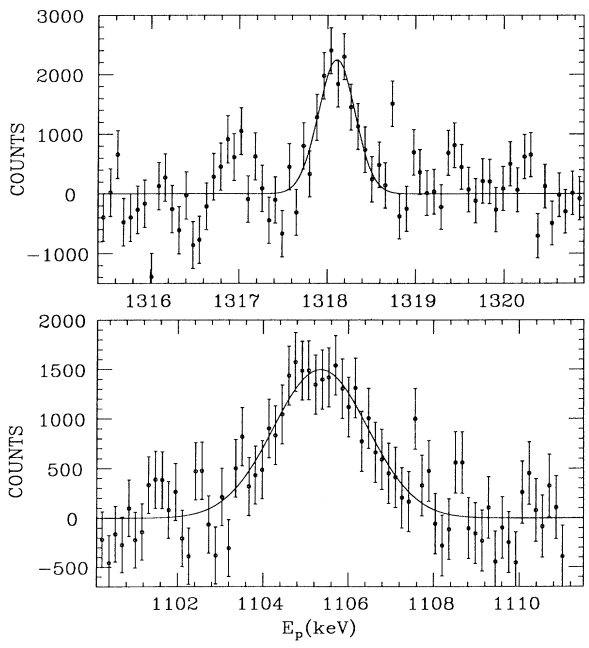

FIG. 13. 1318.1- and 1105.3-keV resonances versus proton energy as observed in the $^{14}C(p,n)^{14}N$ reaction. The counts shown in the figure are the net of original data points less the underlying strong resonance contribution. The solid lines are Gaussian fits to the data.

TABLE IV. Resonances in the $^{14}C(p,n)^{14}N$ reaction.

No.[a]	E_p (keV)[b]	J^{π}[c]	$\Gamma_{c.m.}$ (keV)	$(\omega\gamma)_{c.m.}$ (eV)	E_x (keV)
1	1105.3±1.0	$\geq\frac{3}{2}$	2.4±0.5	(24±4)×10^{-3}	11 238.5±1.0
2	1162.0±1.0	$\frac{1}{2}^-$	5.8±0.3	(0.80±0.07)×10^3	11 291.7±1.0
3	1307.6±1.0	$\frac{1}{2}^+$	d	d	11 427.2±1.0
4	1318.1±1.0	$\frac{7}{2}^-$	<0.4	0.48±0.11	11 437±1.0

[a]Resonances numbered as in Table I.
[b]Energies listed are the observed peak energies less half the target thickness.
[c]From Ref. 21.
[d]The cross section at the peak of the resonance is 0.29±0.02 b. Because this state interferes with the $E_p=1509$ keV ($J^{\pi}=\frac{1}{2}^+$, $T=\frac{3}{2}$) state, $\Gamma_{c.m.}$ and $(\omega\gamma)_{c.m.}$ are not deduced from present work; see Ref. 36. The E_x value for the peak is 8 keV lower than that for the $^{11}B+\alpha$ channel (where the $T=\frac{3}{2}$ level is isospin forbidden), also consistent with the R-matrix analysis in Ref. 36.

gies from the (p,n) threshold at 0.65 to 1.55 MeV. The neutron data for $E_p<1$ MeV are described elsewhere.[27] The cross section of the $^{14}C(p,n)^{14}N$ reaction for $E_p=1-1.55$ MeV is shown in Fig. 12; the two prominent resonances correspond to those numbered 2 and 3 in Table I. The resonance strengths and parameters are shown in Table IV. The results of the present measurements are consistent with the previous work of Morgan[25] on the inverse reaction.

A thinner ^{14}C target (0.28±0.03) $\mu g/cm^2$ was used in conjunction with a 20-kV sawtooth voltage applied to the target to detect the weak resonances expected at $E_p=1104$ and 1316.4 keV (1 and 4 in Table I). The neutron yields of these narrow resonances, after subtracting away the fitted underlying strong resonances, were fitted with Gaussian shapes. The results are shown in Fig. 13. From the area under these fits, the resonance strength for the 1105.3-keV resonance is $(\omega\gamma)_{c.m.}=(24\pm4)$ meV, and that for 1318.1-keV resonance is $(\omega\gamma)_{c.m.}=(0.48\pm0.11)$ eV.

IV. DISCUSSION

A. Resonance structure

Fourteen resonances were observed in the $^{11}B(\alpha,n)^{14}N$ reaction for $E_\alpha=325-2064$ keV (Table I). All but two have been identified previously with the following techniques: neutron-induced reactions or scattering on ^{14}N,[25,28–30] proton elastic scattering or (p,n),(d,n) reactions on ^{14}C,[31–33] (α,n) reactions on ^{11}B,[16–18] or transfer reactions of $^{6,7}Li$ on ^{12}C.[34,35] The J^{π} assignments are shown in Fig. 2 and Table I. The 1458.1-keV resonance (No. 10) is only suggested in the $^{14}C(p,n)^{14}N$ work of Sanders[33] at $E_p\sim2$ MeV (cf. Fig. 4 of Ref. 33), while the 996.0-keV resonance (No. 5) has not been previously reported.

Resonance energies in Table I are consistent with the tabulation of Ajzenberg-Selove[21] except for Nos. 3, 4, 5, 10, and 14. Resonance widths of Nos. 2, 3, 6, 8, 9, 11, and 12 are also consistent with previous work, while the widths of Nos. 1, 7, 13, and 14 are smaller. The energy of the $E_\alpha=2063.7$-keV (No. 14) resonance is 8 keV higher than that from Van der Zwan and Geiger[17] and 26 keV higher than that from Dayras, Switkowski, and Tombrello.[19] (It is interesting to note the presence of two adjacent states in this energy region with same J^{π} but different isospin, with a possible hint of mixing suggested by the slight deviation of the fit in Fig. 2.)

The excitation energy of resonance No. 3 is quoted by Ajzenberg-Selove[21] as $E_x=11\,437.6\pm0.7$ keV, whereas we find 11 435.1±0.7 from (α,n) and 11 427.2±1.0 from the (p,n) resonance peak. As noted in Table IV, the (α,n) vs (p,n) difference is attributed to interference, occurring in the (p,n) reaction only, with another nearby $\frac{1}{2}^+$, isospin $\frac{3}{2}$, level in ^{15}N. It is also to be noted that the position and accuracy of the level as quoted in Ref. 21 are from the R-matrix analysis (ignoring the energy-calibration error) by Ferguson and Gove[36] of the (p,n) data of Bartholomew *et al.*[37] The peak in the original data actually corresponds to $E_x=11\,429\pm3$, in agreement with the present value given above.

The $E_x=11\,436.0$ keV level (No. 4) was first reported by Bommer *et al.*[32] from the $^{14}C(d,n)$ ^{15}N reaction. The (α,n), (α,γ), (α,p) and (p,n) reactions were used here to determine its resonance properties, which are tabulated in Tables V and VI. The neutron width Γ_n is dominant,

TABLE V. $(\omega\gamma)_{c.m.}$ of the $E_x=11.436$ MeV ($J^{\pi}=\frac{7}{2}^-$) state in ^{15}N.

Reaction	$(\omega\gamma)_{c.m.}$(eV)
$^{11}B(\alpha,n)^{14}N$	0.175±0.010
$^{11}B(\alpha,\gamma)^{15}N$	0.021±0.001
$^{11}B(\alpha,p)^{14}C$	0.016±0.001
$^{14}C(p,n)^{14}N$	0.48±0.11

TABLE VI. Partial widths of the $E_x=11.436$ MeV ($J^{\pi}=\frac{7}{2}^-$) state in ^{15}N.

Γ_i	Partial width (eV)
Γ_n	1.69±0.37
Γ_γ	0.20±0.05
Γ_p	0.15±0.04
Γ_α	0.11±0.03
Γ_{total}	2.15±0.38

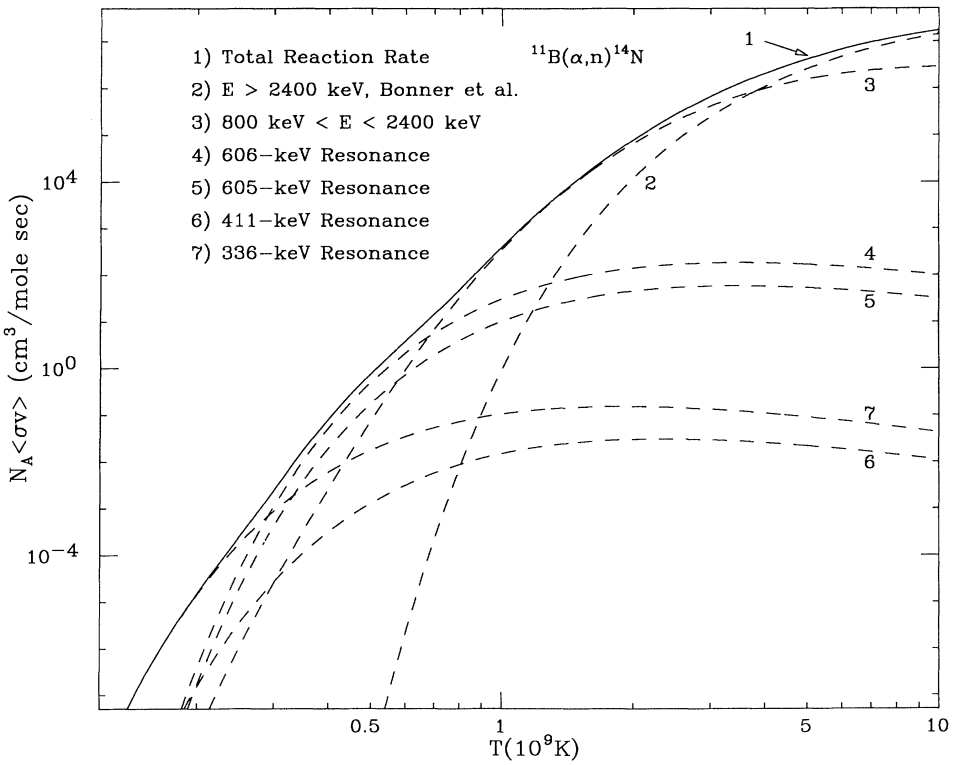

FIG. 14. Reaction rate versus temperature for the $^{11}B(\alpha,n)^{14}N$ reaction. The contributions from various resonances and energy regions are also shown in the figure. The resonance strength of the $E_\alpha=336$-keV resonance is taken from the estimate of Ref. 38. The contribution from the 606-keV resonance dominates for $0.3<T_9<0.7$

while Γ_γ, Γ_p, and Γ_α are comparable in strength. The J^π of this state is determined to be $\frac{7}{2}^-$ (Sec. III. C).

Six resonances were observed in the $^{11}B(\alpha,p)^{14}C$ reaction for $E_\alpha=600-1840$ keV. For $E_\alpha>900$ keV the present results are consistent with the measurements and analysis of Turowiecki *et al.*;[20] below 900 keV no data have been previously reported.

B. Astrophysical implication

The reaction rate $N_A\langle\sigma v\rangle$ of the $^{11}B(\alpha,n)^{14}N$ reaction versus temperature is shown in Fig. 14. The required data beyond our measured range ($E_\alpha>2400$ keV were taken from the work of Bonner *et al.*[16] The resonance strength of the 336.7-keV resonance was taken from the estimate of Caughlan and Fowler.[38] Using their conventional formulation, the fitted reaction rate for the $^{11}B(\alpha,n)^{14}N$ reaction can be expressed as

$$N_A\langle\sigma v\rangle=2.468\times10^{15}(1+7.519T_9^{1/3}+1.361T_9^{2/3}-14.972T_9-11.61T_9^{4/3}+18.145T_9^{5/3})$$
$$\times\exp\left[-\frac{18.145}{T_9^{1/3}}-\left[\frac{T_9}{0.7207}\right]^2\right]+1.459\times10^7T_9^{3/5}\exp\left[-\frac{11.26}{T_9}\right]$$
$$+\frac{1.79}{T_9^{3/2}}\exp\left[-\frac{2.868}{T_9}\right]+\frac{1.678\times10^3}{T_9^{3/2}}\exp\left[-\frac{5.147}{T_9}\right]+\frac{5.358\times10^3}{T_9^{3/2}}\exp\left[-\frac{5.157}{T_9}\right]. \quad (4)$$

The fit is better than 2% for $T_9>0.1$ except for the region around $T_9=1.2$, where the discrepancy between the data and Eq. (4) is 12%. As shown in Fig. 14, for $T_9=0.28-0.65$, $N_A\langle\sigma v\rangle$ is dominated by the $E_\alpha=606$-keV resonance. For $T_9<0.28$ the contribution from 336.7-keV resonance dominates.

The reaction rate for the $^{11}B(\alpha,p)^{14}C$ reaction versus temperature is shown in Fig. 15. The required data for $E_\alpha>1820$ keV were taken from Dayras, Switkowski, and Tombrello.[19] The resonance strength of the 336.7-keV resonance was again taken from Caughlan and Fowler.[38] The fitted reaction rate for the $^{11}B(\alpha,p)^{14}C$ reaction can be expressed as

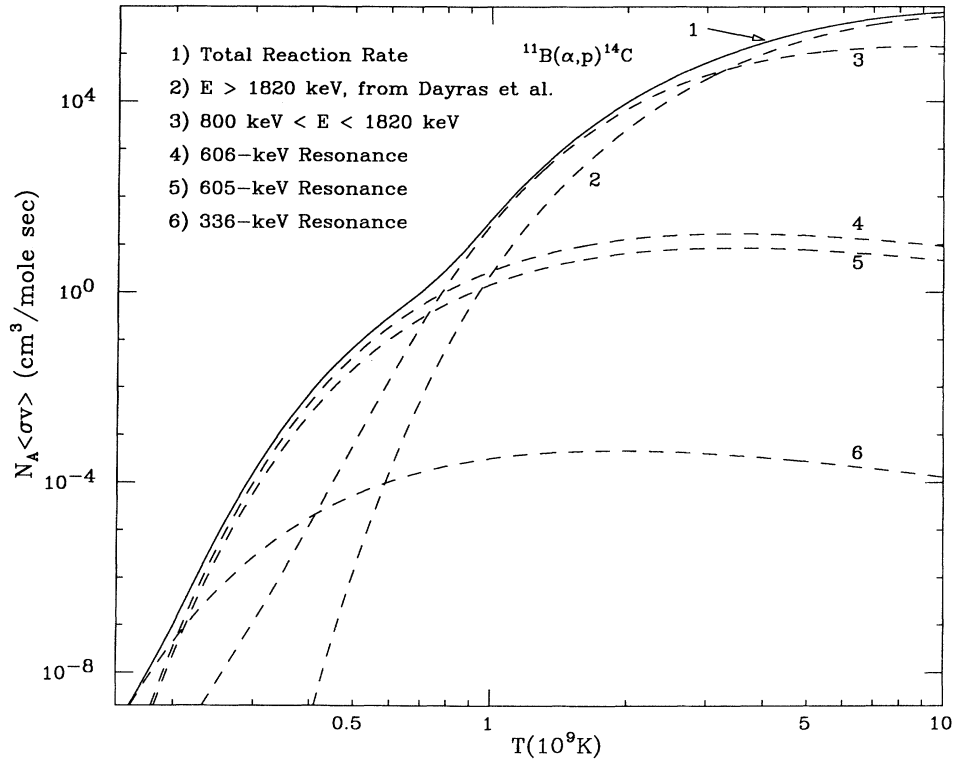

FIG. 15. Reaction rate versus temperature for the $^{11}B(\alpha,p)^{14}C$ reaction. The contributions from various resonances and energy regions are also shown in the figure. The resonance strength of the $E_\alpha = 336$-keV resonance is taken from the estimate of Ref. 38. The contribution from the 606-keV resonance dominates for $0.2 < T_9 < 0.8$.

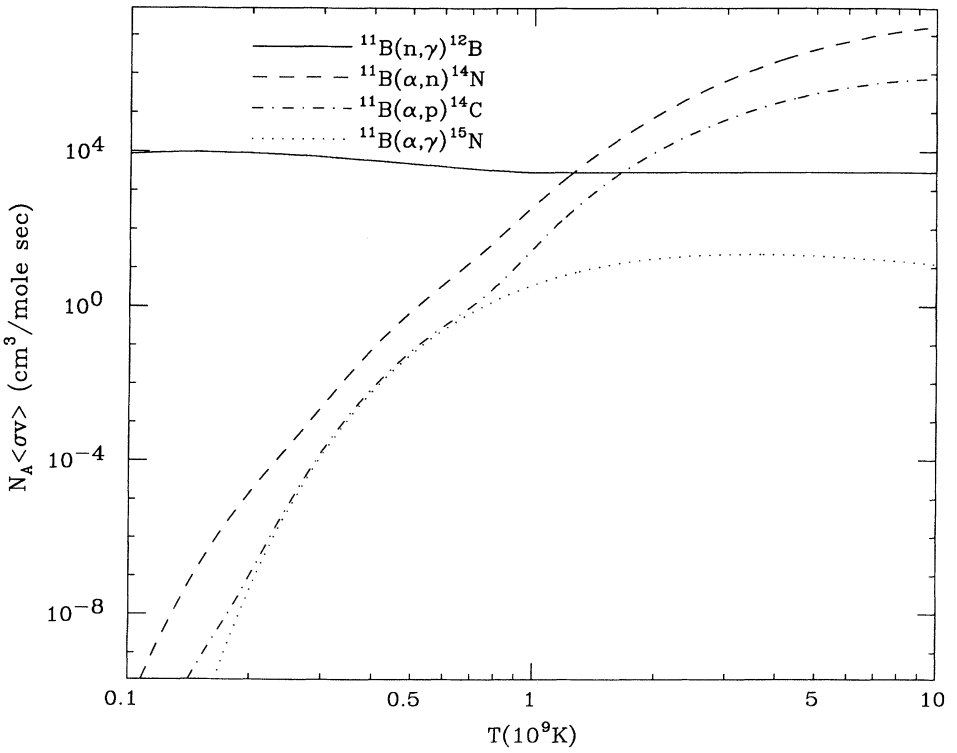

FIG. 16. Comparison of the reaction rates for $^{11}B(n,\gamma)^{12}B$ to various $^{11}B+\alpha$ reactions. The $^{11}B(\alpha,n)^{14}N$ rate exceeds that for $^{11}B(n,\gamma)^{12}B$ for $T_9 > 1.2$

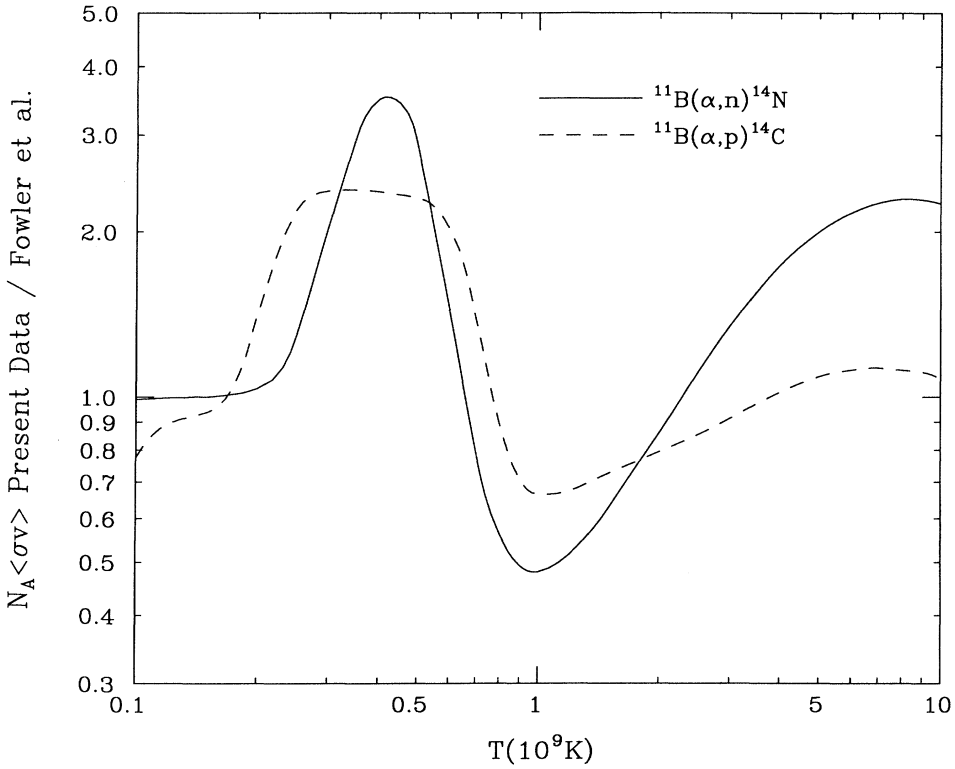

FIG. 17. Ratio of the experimental reaction rates of the ^{11}B(α,n)^{14}N and ^{11}B(α,p)^{14}C reactions to the rates given in Ref. 38. The enhancement of the ratio for $T_9 \sim 0.4$ is due to the contribution of the 606-keV resonance.

$$N_A\langle\sigma v\rangle = 8.403\times10^{15}(1+0.022T_9^{1/3}+5.712T_9^{2/3}+0.642T_9+15.982T_9^{4/3}+4.062T_9^{5/3})$$
$$\times\exp\left[\frac{-31.914}{T_9^{1/3}}-\left[\frac{T_9}{0.3432}\right]^2\right]+4.944\times10^6T_9^{3/5}\exp\left[-\frac{11.26}{T_9}\right]$$
$$+\frac{5.44\times10^{-3}}{T_9^{3/2}}\exp\left[-\frac{2.868}{T_9}\right]+\frac{2.419\times10^2}{T_9^{3/2}}\exp\left[-\frac{5.147}{T_9}\right]+\frac{4.899\times10^2}{T_9^{3/2}}\exp\left[-\frac{5.157}{T_9}\right]. \quad (5)$$

The fit is better than 10% for $T_9 > 0.1$ except in the region around $T_9 = 4$, where the discrepancy between data and Eq. (5) is 14%. As shown in Fig. 15, the reaction rate for $T_9 = 0.2$–0.75 is again dominated by the 606-keV resonance, while the contribution from the 605-keV resonance amounts to $\sim\frac{1}{2}$ of the contribution from the 606-keV resonance. The reaction rate for $T_9 < 0.2$ is dominated by the 336.7-keV resonance.

Comparison of the reaction rates for the various ^{11}B+α reactions is shown in Fig. 16. The reaction rate for ^{11}B(α,γ) is from the 606-keV resonance contribution only; other resonances are expected to contribute negligibly. The reaction rate for ^{11}B(n,γ)^{12}B reaction is dominated at low T_9 by the known 20.8-keV resonance;[39] including also the thermal term (from $\sigma_{\rm th} = 5.5$ mb) and data[21] for the next four higher resonances, the fitted rate is

$$N_A\langle\sigma v\rangle = 729+\frac{2.25\times10^3}{T_9^{3/2}}\exp\left[-\frac{0.221}{T_9}\right]+\frac{3.26\times10^4}{T_9^{3/2}}\exp\left[-\frac{4.514}{T_9}\right]+\frac{1.96\times10^4}{T_9^{3/2}}\exp\left[-\frac{10.804}{T_9}\right]$$
$$+\frac{3.90\times10^4}{T_9^{3/2}}\exp\left[-\frac{13.323}{T_9}\right]+\frac{5.86\times10^4}{T_9^{3/2}}\exp\left[-\frac{18.916}{T_9}\right]. \quad (6)$$

The actual rates in the first few minutes of nucleosynthesis in the early Universe depend on the time-dependent reactant densities. In typical models the ^{4}He density exceeds the neutron density for $t \geq 200$ s, when $T_9 \leq 0.9$. As shown in Fig. 16, for $T_9 < 1.2$, the most interesting temperature region in primordial nucleosynthesis, the ^{11}B(n,γ)^{12}B reaction

dominates, consistent with the reaction sequence proposed by Malaney and Fowler.[7] For $T_9 = 1.2-10$ the reaction rate for $^{11}B(\alpha,n)$ dominates. It is interesting to note that $^{11}B(\alpha,\gamma)$ is comparable to $^{11}B(\alpha,p)$ for $T_9 < 0.7$, producing ^{15}N directly.

The $N_A\langle\sigma v\rangle$ for $^{11}B+\alpha$ reactions are compared with the rates from Ref. 38 in Fig. 17. The main difference is from the contribution of the 606-keV resonance, most significant in the range for $T_9 = 0.3-0.7$. Although the reaction rates differ from those of Ref. 38 by as much as a factor of 4 in this region, the difference is not large enough to change the principal reaction sequence in primordial nucleosynthesis as presently formulated.

ACKNOWLEDGMENTS

We thank W.A. Fowler and R.E. Azuma for many useful discussions during the course of this work, and S.E. Kellogg for help during the experiments. This work is supported by the National Science Foundation Grant Nos. PHY85-05682 and PHY88-17296.

[1]E. Witten, Phys. Rev. D **30**, 272 (1984).
[2]J. H. Applegate and C. J. Hogan, Phys. Rev. D **31**, 3037 (1985).
[3]C. R. Alcock, G. M. Fuller, and G. J. Mathews, Astrophys. J. **320**, 439 (1987).
[4]G. M. Fuller, G. J. Mathews, and C. R. Alcock, Phys. Rev. D **37**, 1380 (1988).
[5]J. H. Applegate, C. J. Hogan, and R. J. Scherrer, Phys. Rev. D **35**, 1151 (1987).
[6]J. H. Applegate, C. J. Hogan, and R. J. Scherrer, Astrophys. J. **320**, 439 (1988).
[7]R. A. Malaney and W. A. Fowler, in *Origin and Distribution of the Elements*, edited by G. J. Mathews (World Scientific, Singapore, 1988), p. 76.
[8]R. A. Malaney and W. A. Fowler, Astrophys. J. **333**, 14 (1988).
[9]F. Spite and M. Spite, Astron. Astrophys. **115**, 357 (1982).
[10]M. Spite, J. P. Maillard, and F. Spite, Astron. Astrophys. **141**, 56 (1984).
[11]J. Yang, M. S. Turner, G. Steigman, D. N. Schramm, and K. A. Olive, Astrophys. J. **281**, 493 (1984).
[12]R. N. Boyd and T. Kajino, Astrophys. J. **336**, L55 (1989).
[13]R. Rebolo, P. Molaro, C. Abia, and J. E. Beckman, Astron. Astrophys. **193**, 192 (1988). For ^{9}Be observations, see also S. G. Ryan, M. S. Bessell, R. S. Sutherland, and J. E. Norris, Astrophys. J. Lett. **348**, L57 (1990).
[14]R. A. Malaney, in *Workshop on Primordial Nucleosynthesis*, (World Scientific, Singapore, 1989), p. 49.
[15]T. Paradellis, S. Kossionides, G. Doukellis, X. Aslanoglou, P. Assimakopoulos, A. Pakou, C. Rolfs, and K. Langanke, Z. Phys. A **337**, 211 (1990).
[16]T. W. Bonner, A. A. Kraus Jr., J. B. Marion, and J. P. Schiffer, Phys. Rev. **102**, 1348 (1956).
[17]L. Van der Zwan and K. W. Geiger, Nucl. Phys. **A246**, 93 (1975).
[18]M. Niecke, M. Niemeier, R. Weigel, and H. Wirzba-Lorenz, Nucl. Phys. **A289**, 408 (1977).
[19]R. A. Dayras, Z. E. Switkowski, and T. A. Tombrello, Nucl. Phys. **A261**, 365 (1976).
[20]A. Turowiecki, A. Saganek, M. Sieminski, E. Wesolowski, and Z. Wilhelmi, Nucl. Phys. **A468**, 29 (1987).
[21]F. Ajzenberg-Selove, Nucl. Phys. **A449**, 1 (1986).
[22]R. T. Skelton, R. W. Kavanagh, and D. G. Sargood, Astrophys. J. **271**, 404 (1983).
[23]S. E. Kellogg and R. W. Kavanagh, Bull. Am. Phys. Soc. **34**, 1192 (1989); (unpublished).
[24]R. B. Vogelaar, Ph.D. thesis, California Institute of Technology, 1989 (unpublished).
[25]G. L. Morgan, Nucl. Sci. Eng. **70**, 163 (1979).
[26]J. E. Ziegler, *Helium Stopping Powers and Ranges in All Elements* (Pergamon, New York, 1977).
[27]S. E. Kellogg, R. B. Vogelaar, and R. W. Kavanagh, Bull. Am. Phys. Soc. **34**, 1192 (1989); (unpublished).
[28]C. H. Johnson, B. Petree, and R. K. Adair, Phys. Rev. C **84**, 775 (1951).
[29]C. H. Johnson and H. H. Barschall, Phys. Rev. **80**, 818 (1950).
[30]J. J. Hinchey, P. H. Stelson, and W. M. Preston, Phys. Rev. **86**, 483 (1952).
[31]W. D. Roseborough, J. J. G. McCue, W. M. Preston, and C. Goodman, Phys. Rev. **83**, 1133 (1951).
[32]J. Bommer, M. Ekpo, H. Fuchs, K. Grabisch, and H. Kluge, Nucl. Phys. **A251**, 246 (1975).
[33]R. M. Sanders, Phys. Rev. **104**, 1434 (1956).
[34]I. Tserruya, B. Rosner, and K. Bethge, Nucl. Phys. **A213**, 22 (1973).
[35]H. G. Bingham, M. L. Halbert, D. C. Hensley, E. Newman, K. W. Kemper, and L. A. Charlton, Phys. Rev. C **11**, 1913 (1975).
[36]A. J. Ferguson and H. E. Gove, Can. J. Phys. **37**, 660 (1959).
[37]G. A. Bartholomew, F. Brown, H. E. Gove, A.E. Litherland, and E. B. Paul, Can. J. Phys. **33**, 441 (1955).
[38]G. R. Caughlan and W. A. Fowler, At. Data Nucl. Data Tables **40**, 299 (1988).
[39]F. P. Mooring, J. E. Monahan, and R. E. Segel, Phys. Rev. **178**, 1612 (1969).